Proton Component of the Primary Cosmic Radiation*

FRANK B. MCDONALD,† *State University of Iowa, Iowa City, Iowa*

AND

WILLIAM R. WEBBER, *Imperial College, London, England*

(Received January 14, 1959)

The proton component has been extensively studied at high altitudes on a series of 6 Skyhook balloon flights at various latitudes using the Čerenkov-scintillation counter technique. The intensity of primary protons has been measured at 4°, 41°, 53°, and 55° geomagnetic latitude. The proton differential energy spectrum has been measured directly in the region 250–750 Mev. It is observed that primary alphas and protons have the same form of rigidity spectrum from 1 Bv to 17 Bv. A series of cutoff rigidities are measured in the vicinity of $\lambda=53°$ and 55°. The intensity and composition of fast splash albedo is determined at $\lambda=4°$, 53°, and 55°. Significant time variations are observed between the three high-latitude flights. Differences observed in the intensity and energy spectra of these three flights are discussed and strong restraints are placed on possible modulating mechanisms.

I. INTRODUCTION

THE task of measuring primary cosmic-ray flux values is much more difficult for protons than for multiply charged particles. The interaction of primaries with air nuclei produces many fast, singly charged secondaries. Some of these secondaries move in an upward direction and constitute the "splash albedo." The earth's magnetic field acts on the splash albedo and a portion of it will re-enter the earth's atmosphere and constitute the "returning albedo." The copious production of fast secondaries, which are difficult to distinguish from primary protons, and the albedo problem greatly complicate the determination of the primary proton intensity and energy spectrum.

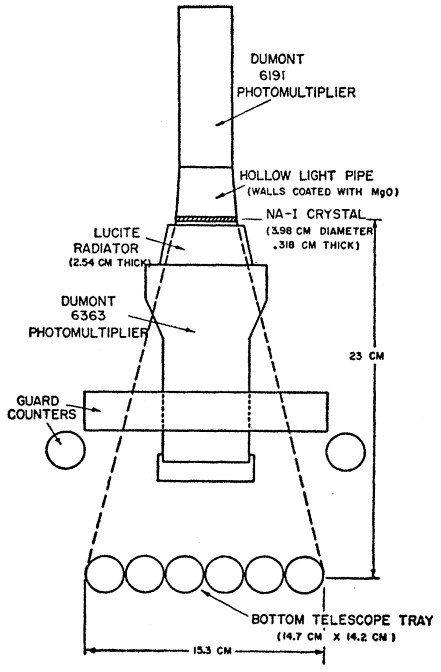

FIG. 1. Outline drawing of Čerenkov-scintillation counter telescope. Telescope contains 8.8 g/cm² (air equivalent) of material.

Recent experiments using ionization-type detectors in conjunction with varying thicknesses of absorbing materials[1–3] to separate the primaries and secondaries into various energy intervals, and other experiments using Čerenkov detectors to separate the downward moving primaries and secondaries from the "splash albedo,"[4] have greatly increased our knowledge of the singly charged component at high altitudes.

The Čerenkov-scintillator technique developed at the State University of Iowa[5] combines the best attributes of both types of detectors to become a powerful tool for the investigation of the singly charged component as well as the multiply charged components of the primary radiation at balloon altitudes.

The combination of the two detectors gives charge resolution which is independent of velocity. In addition, *two* measurements of velocity and/or direction serve effectively to separate and identify three general groups of singly charged particles. These are: (1) Fast particles (FP) with $\beta \gtrsim 0.83$ (proton kinetic energy, $E_p \geqq 750$ Mev). At balloon altitudes this group of particles consists mostly of primary protons with an additional small percentage of mesons and electrons. (2) Fast splash albedo (FSA) with $\beta \gtrsim 0.7$, consisting mostly of electrons but also including an appreciable fraction of higher energy protons or mesons. (3) Slow particles (SP) with $0.44 \leq \beta \leq 0.83$ ($100 \leq$ proton kinetic energy, $E_p \leq 750$ Mev). At balloon altitudes it will be shown that these particles are almost all protons. Below $\beta=0.7$ ($E_p \geqq 320$ Mev), it is impossible to distinguish

* Assisted by the joint program of the Office of Naval Research and the U. S. Atomic Energy Commission.

† Now at National and Aeronautics and Space Administration's Goddard Space Center, Washington, D. C.

[1] Perlow, Davis, Kissinger, and Shipman, Phys. Rev. **88**, 321 (1952).
[2] Davis, Caulk, and Johnson, Phys. Rev. **101**, 800 (1956).
[3] G. W. McClure, Phys. Rev. **96**, 1391 (1953).
[4] J. R. Winckler and K. Anderson, Phys. Rev. **93**, 596 (1954).
[5] F. B. McDonald, Phys. Rev. **104**, 1723 (1956).

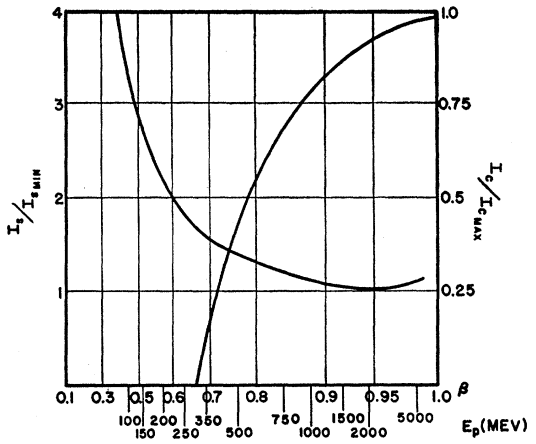

FIG. 2. Čerenkov-scintillation counter output as a function of velocity and energy. The top scale of abscissa is the velocity of the incident particle, and the two lower scales represent the corresponding proton kinetic energy, E_p. I_c is zero at 320 Mev.

the direction of these protons. The slow-particle group lies in the effective energy-sensitive region of the detectors and it is possible to determine directly the energy spectra of these particles.

The Čerenkov-scintillation detector provides a means of measuring the absolute intensity of singly charged particles with $\beta>0.83$. Methods will be described for the extrapolation of the balloon data to the top of the atmosphere. It is possible to determine directly the intensity and energy spectra of primary protons in the region 150–750 Mev. Thus one can measure geomagnetic cutoff energies and differential primary spectra for protons in this energy region. It is also an excellent method for studying the energy dependence of time variations of the primary radiation.

II. DESCRIPTION OF THE APPARATUS

The Čerenkov-scintillation counter used was identical to that previously described.[5] Briefly, the detector is a three-element telescope (Fig. 1) consisting of a NaI crystal scintillation counter, a Lucite Čerenkov counter, a tray of Geiger counters and a system of guard counters. A coincidence is recorded when a particle traverses the scintillation crystal and the lower tray of Geiger counters. In addition, a notation is made if more than one counter in the bottom tray or if one of the system of guard counters is triggered in conjunction with a telescope event. Such events are called "multiple counts" as opposed to the unaccompanied particles which produce "regular counts."

For each particle that triggers the telescope, the pulse heights from the Čerenkov counter and the scintillation counter are recorded. These pulse heights are translated into deflections of spots on two cathode-ray tubes and the resulting traces are recorded on a continuously moving film with an accurate time base superimposed.

III. PRESENTATION OF DATA

The relationship between the measured pulse heights of the traces produced by the outputs from the Čerenkov and scintillation detectors should uniquely determine the velocity and direction of the particle in question. The relations between the output of the scintillation counter (I_s) and the output of the Čerenkov counter (I_c) as a function of the velocity of the incident particle are shown in Fig. 2. Also shown is the proton kinetic energy as a function of this velocity.

If the data obtained at maximum altitude during a typical balloon flight are recorded on a suitable two-dimensional data grid with one axis representing I_c and the other I_s, the picture shown in Fig. 3 emerges. The explanation of the regions is as follows:

(*1*) *Fast particles* (FP).—If the gains of the electronic system are suitably chosen, the outputs I_c and I_s from highly relativistic ($\beta\sim1$) particles should be identical. The position $I_{c\,\max}$, $I_{s\,\min}$ marks the center of the fast-particle region. In the case of the Čerenkov detector, the scatter about this point is due primarily to the statistical fluctuations in the output of the viewing phototube. In the case of the scintillation counter, the fluctuations in the output I_s are mainly due to the statistical fluctuations in the energy loss by ionization in thin materials (Landau effect). The line L represents this fact, i.e., that occasional large energy losses can occur which will distort the distribution of energy losses, especially when the average energy loss is small.

Fortunately, sea-level cosmic-ray μ mesons provide a provide a convenient source of high velocity ($\beta>0.98$) particles for checking the response of the apparatus. The line bounding the fast-particle region represents the position at which the intensity of counts has dropped to 15% of that at the center of the fast-particle

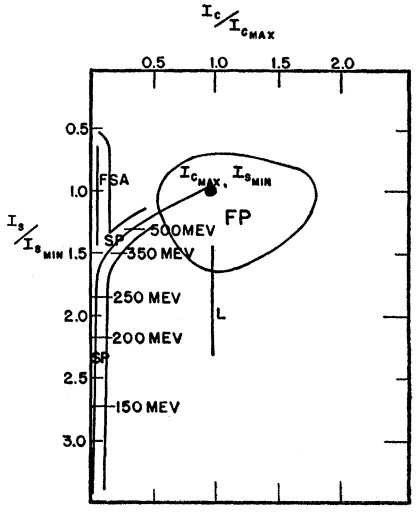

FIG. 3. Schematic picture of two-dimensional data grid for singly charged particles. (See text for definition of symbols.)

distribution according to sea-level μ-meson tests (closely corroborated by fast-particle distributions obtained at balloon altitudes). The Landau "tail" is observed for sea-level μ mesons and is identical with that obtained for fast particles at altitude.

(*2*) *Slow particles* (SP).—The line labeled SP represents the center of the region in which particles with $0.44 \leq \beta \leq 0.83$ would be expected to lie on the data grid. The following arguments convince one that the counts in this region must indeed be predominantly slow protons. (a) In order to penetrate the detector, electrons must have $\beta \sim 1$. (b) In order to penetrate the detector, mesons must have $\beta \geq 0.7$. However, the number of mesons with $0.7 \leq \beta \leq 0.83$ ($40 \leq E \leq 80$ Mev) is negligible compared with the number of protons in this range ($360 \leq E_p \leq 750$ Mev) at balloon altitudes.

The energy calibration in the slow-particle region is based on the fact that the center of the FP distribution represents the position $I_{s\,\min}$, $I_{c\,\max}$.

(*3*) *Fast splash albedo* (FSA).—The counts lying along FSA will represent the fast splash albedo ($\beta \geq 0.70$) ($E_p \leq 320$ Mev), as the Čerenkov response for upward moving particles is much less than that for downward moving particles. This is due to the directional properties of the Čerenkov radiation, whereas the response of the scintillation counter is independent of the direction the particle traverses the telescope.

Splash albedo particles with $\beta \leq 0.70$ will be indistinguishable from downward moving particles of the same velocity from the data obtained at any one given altitude. However, if one analyzes the altitude dependence of these events between 5 and 50 g/cm^2, it is possible to separate the two components.

IV. REDUCTION OF RAW DATA

The procedures used in determining the intensities and/or energy spectra of the FP, FSA, and SP components are discussed in the following sections:

(*a*) *Fast particles.*—A typical two-dimensional distribution consisting primarily of fast particles can be obtained by studying the response of the detector to cosmic rays at sea level. The sea-level two-dimensional grids are first normalized to and then subtracted from the comparable grids for the altitude portions of the flights. (Normalization procedure requires that the number of counts in the region $0.6\,I_{c\,\max} \leq I_c \leq 1.5\,I_{c\,\max}$, $0.6\,I_{s\,\min} \leq I_s \leq 1.5\,I_{s\,\min}$ are equal for the respective data grids.) The normalized sea-level data grid then gives the uncorrected number of FP counts for the particular altitude interval. The residual counts in the altitude distributions then consist of (1) SP counts, (2) FSA counts, and (3) background counts due to nuclear interactions and showers not recorded by the multiple-particle detection system. As will be discussed later, the number of background counts in the normalization interval is small ($<5\%$ of the regular counts) and can be estimated as well as evaluated from the experimental data.

The following corrections must now be applied to the FP intensity obtained by the above procedure in order to obtain the intensity of FP incident on the detector.

(1) A δ-ray correction is necessary, as it is possible for particles traversing the top elements of the telescope to produce knock-on electrons which will trigger one of the Geiger counters. This results in the particles which would normally pass through the telescope being classified as multiple-particle counts. Some particles which miss the bottom element will appear as regular counts and there will be a corresponding spurious increase of the geometric factor. Details of this calculation have been given by Webber[6] for a telescope with similar geometry and multiple-particle detection system. The correction due to this effect amounts to $+1.5\%$ for particles in this velocity range ($\beta \geq 0.83$). It is negligible for particles of lower velocity.

(2) A correction for protons in the FP distribution which have interacted as they pass through the telescope (8.8 g/cm^2 of material) is also necessary. The events could be recorded either as multiple particle counts or as "background" regular counts depending on the efficiency (K) of the multiple-particle detection system. Because of the normalization procedure used in obtaining the number of FP counts, the interactions recorded as "background" regular counts were included as part of the FP distribution. Therefore we must add $\{1-(1-K)\}[1-\exp(-8.8/\lambda_p)]J_p$ counts, where J_p is the number of fast protons (taken to be the number of FP counts) and λ_p is their interaction mean free path. In this correction we have assumed that every interaction of these energetic protons will produce at least one particle capable of reaching the bottom telescope element.

The efficiency of the multiple-particle detection system (K) can be evaluated from the experimental data. This is found to be 0.5 ± 0.1 for all flights. It is important to note that the magnitude of these corrections is small and in both cases is less than 6%.

(*b*) *Fast splash albedo.*—We shall assume here (to be discussed in more detail later) that most of the fast splash albedo consists of electrons ($\beta \sim 1$). Corrections due to δ rays and nuclear interactions thus will not exist. Instead, however, we have a correction for "background" events lying in the regular fast albedo region that were not detected by the multiple-particle detection system. Since these counts are not due to albedo particles, we must subtract them from the fast splash albedo counts. This correction amounts to $-[(1-K)/K]$ times the number of multiple-particle counts lying in the fast albedo region. For fast splash albedo counts there is also a further correction due to the Landau effect which permits particles with $\beta \simeq 1$ to have energy losses greater than $1.35\,I_{s\,\min}$.

[6] W. R. Webber, Nuovo cimento 4, 1285 (1956).

TABLE I. Summary of corrections to raw data.

Type of particle	Type of correction			
	δ rays	Nuclear interactions[a]	Landau	Background
Fast particles	$0.015J_{FP}$	$K[1-\exp(-8.8/\lambda p)]J_p$ $=(0.06\pm0.01)J_p$	None	See nuclear interactions
Slow protons				
100–150 Mev		$(0.12\pm0.04)J_{125}$	$-(0.00\pm0.01)J_{FSA}$ $-(0.04\pm0.02)J_{125}$	
150–200 Mev		$(0.10\pm0.04)J_{175}$	$-(0.01\pm0.01)J_{FSA}$ $-(0.13\pm0.04)J_{175}$	$-[(1-K)/K]\times$MPE[b]
200–250 Mev	None	$(0.08\pm0.03)J_{225}$	$-(0.02\pm0.01)J_{FSA}$ $-(0.08\pm0.04)J_{225}$	
250–350 Mev		$(0.06\pm0.03)J_{sp\ 300}$	$-(0.06\pm0.02)J_{FSA}$ $+(0.22\pm0.06)J_{300}$	$=(1.0\pm0.3)\times$MPE
350–500 Mev		$(0.03\pm0.02)J_{sp\ 425}$	$-(0.05\pm0.02)J_{FSA}$ $+(0.45\pm0.15)J_{425}$	
500–750 Mev		$(0.00\pm0.02)J_{sp\ 625}$	$+(0.00\pm0.00)J_{FSA}$ $+(0.60\pm0.20)J_{625}$	
Fast splash albedo	None	None	$+(0.20\pm0.05)J_{FSA}$ $-(0.15\pm0.05)J_{250-500}$	$-[(1-K)/K]\times$MPE $=-(1.0\pm0.3)\times$MPE

[a] $\lambda p = 70$ g/cm².

[b] MPE = Multiple particle events.

(*c*) *Slow particles.*—The center of the FP distribution serves to determine the position $I_{s\ \min}$, $I_{c\ \max}$ and therefore to calibrate the energy response of the detector. This position is quite accurately defined and is known to within ±5% (see reference 5 for a more complete description of the energy calibrations).

Based on the known energy loss *vs* energy curves, the slow proton distribution is divided into six energy intervals from 100 Mev to 750 Mev. Due to the uncertainty in the position $I_{s\ \min}$, $I_{c\ \max}$ these energies are known to within $<\pm10\%$.

The number of slow protons assigned to the various energy intervals must be corrected for the following effects in order to obtain the intensities of slow protons nc ident on the detector.

(*a*) *Nuclear interactions.*—From the work of Camerini *et al.*[7] on secondaries from interactions of protons with 100 Mev$\leqq E\leqq$750 Mev, we can conclude that the number of secondaries capable of penetrating the lower counters ranges between 0.2 and 1.0 per interaction depending on the energy of the primary. Most of the interacting protons will thus produce regular counts or no counts at all, with very few multiple counts being obtained.

An empirical correction has been derived from this work and amounts to at most a 10% correction to the number of counts in each energy interval.

(*b*) *Background events.*—These events will lie in the regular slow proton distribution due to the inefficiency of the multiple-particle detection system. Since these events are not due to slow protons, they must be subtracted from the slow proton events. As with the splash albedo correction, this amounts to $-[(1-K)/K]$ times the number of multiple-particle events lying in the various slow proton energy intervals.

(*c*) *Landau effect.*—In order to derive an energy spectrum for the slow protons, it is necessary to relate the observed number of particles within an interval of energy loss to the actual number in that interval expected in the absence of energy loss fluctuations. A complete solution to the problem of fluctuations of ionization loss in thin absorbers has been carried out by Symon.[8] Using his results, it has been possible to synthesize the actual energy distribution of slow protons.

The corrections due to this effect are listed in Table I for the various energy intervals. Table I also gives a summary of the various corrections discussed above.

V. BALLOON FLIGHTS

The data on which this report is based come from six balloon flights using the Čerenkov-scintillation detector. These flights were made during the period January, 1955 to August, 1956. They include one flight at $\lambda=4°$, two at $\lambda=41°$, one at $\lambda=53°$ and two at $\lambda=55°$. The time-altitude records and location, as well as the dates of these flights, are shown in Fig. 4(a). Figure 4(b) shows the trajectories of the $\lambda=53°$, and 55° flights. Also drawn in this figure are lines of geomagnetic latitude and lines of equal cutoff momentum as given by Quenby and Webber.[9] The primary cosmic-ray alpha data from these flights have been previously reported.[10]

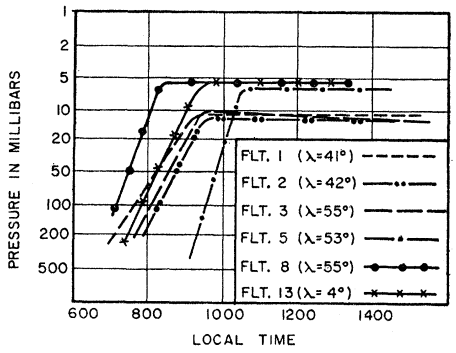

FIG. 4(a). Time altitude record of balloon flights. Flights 1 and 2 were launched from San Angelo, Texas ($\lambda=41°$). Flights 3 and 8 were launched from Minneapolis, Minnesota ($\lambda=55°$). Flight 5 was launched from Iowa City, Iowa ($\lambda=53°$), and Flight 13 was launched from Guam, Mariana Islands ($\lambda=4°$).

[7] Camerini, Davies, Fowler, Franzinetti, Lock, Perkins, and Yekutieli, Phil. Mag. **42**, 1241 (1951).

[8] K. R. Symon, thesis, Harvard University, 1948 (unpublished).

[9] J. J. Quenby and W. R. Webber, Phil. Mag. (to be published).

[10] F. B. McDonald, Phys. Rev. **109**, 1367 (1958).

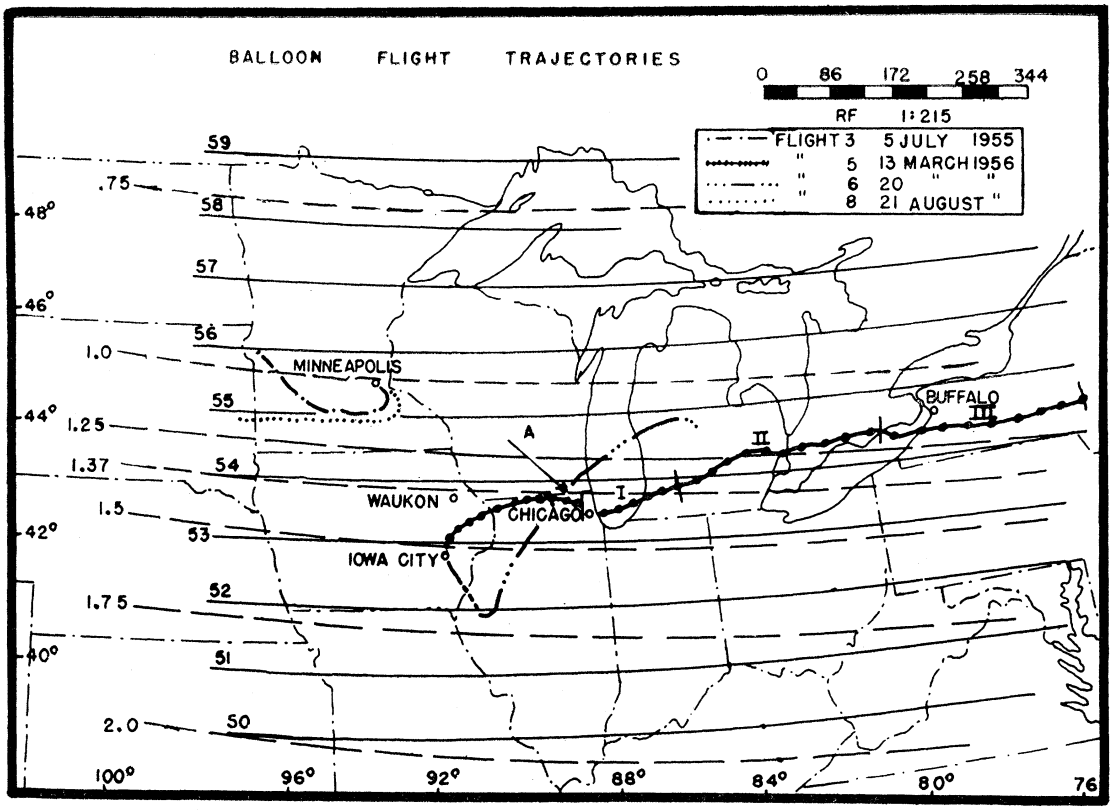

FIG. 4(b). Trajectory for high-latitude flights. The solid curves represent geomagnetic latitude while the dotted lines represent lines of constant cutoff rigidities, measured in Bv as calculated by Quenby and Webber.[9] Point *A* represents the point on Flight 6 (launched March 20, 1956) where an accurate α-particle cutoff energy was measured. Note that Flight 5 is divided into three intervals; I, II, and III. This is necessary because this flight moved through 2° geomagnetic latitude and because significant time variations occur during the course of the flight.

VI. BALLOON FLIGHT DATA

The data obtained during the rising portions of the balloon flights and at maximum altitude were analyzed in 15-minute intervals. This permitted a close check on possible gain changes in the equipment as well as actual primary intensity variations.

Figure 5 shows a simplified two-dimensional data grid of regular counts for the total high-altitude portion of Flight 13 ($\lambda=4°$). Figure 6(a) shows the corresponding data grid obtained at sea level. And finally 6(b) shows the sea level "albedo" data grid. (Number of counts and position $I_{s\,\min}$, $I_{c\,\max}$ are normalized for the various distributions.) Note the clear-cut separation of the splash albedo and slow proton counts in the distributions at maximum altitude and the corresponding absence of such counts in the sea-level distribution.

The data shown in Figs. 7 and 8 summarize the results of all the flights. Figure 7 shows the altitude dependence of the corrected fast-particle intensity for various latitudes. Figure 8 shows the corresponding data for slow particles.

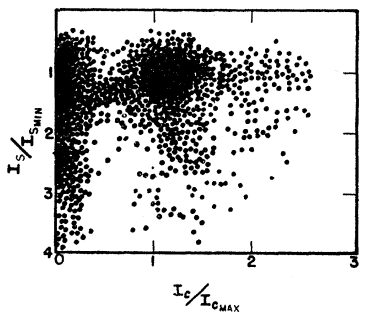

FIG. 5. Two-dimensional data grid obtained on Flight 13 ($\lambda=4°$) at 5 g/cm². Each dot represents a single count. There are approximately 1500 counts in the fast-particle region.

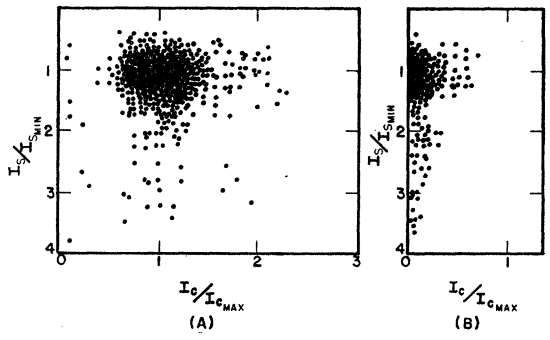

FIG. 6(a) Two-dimensional data grid obtained at sea level. (b) Two-dimensional data grid obtained at sea level with apparatus inverted.

TABLE II. Vertical primary proton intensities at the top of the atmosphere.

Flt. No.	Date	Geomagnetic latitude	Cutoff rigidity (calculated by Quenby-Webber method[a]) R_m in Bv	Cutoff energy E_m, Bev corresponding to R_m	FP at 15 g/cm² particles/ m²-sec-sterad	FP at 5 g/cm² particles/ m²-sec-sterad	Primary protons with energy greater than geomagnetic cutoff energy, E_m, or 750 Mev (whichever is larger) +re-entrant albedo at 0 g/cm² in particles/ m²-sec-sterad
13	1–30–57	4°	17.0	16.1	215±10	145±5	115±10
1	1–17–55	41.8°	4.6	3.8	1030±20		630±40
2	1–22–55	42.4°	4.3	3.5	1065±15		650±40
5	3–13–56(1)	53.0°	1.4	0.8	1880±50	1700±40	1600±50
	(2)		1.3	0.670		1820±30	1720±50
	(3)		1.1			1945±30	1850±50
3	7– 7–55	55.3°	1.1	0.50	2500±40		2240±50
8	8–21–56	54.9°	1.2	0.55	2050±40	1910±20	1820±50

[a] See reference 9.

VII. INTENSITIES OF PRIMARY PROTONS

As has been pointed out previously, the intensity of fast particles at any given high altitude will consist principally of primary protons which have not interacted with the air nuclei. However, there will be an appreciable fraction of mesons, electrons and fast secondary protons present in this distribution also, due to the protons that have already interacted. The best method of correcting for the production of these fast secondaries above the telescope is to extrapolate the intensity-altitude curves for FP to the top of the atmosphere. This will effectively "subtract" the secondary particles and give the intensity of primary protons (plus re-entrant albedo) at the top of the atmosphere. The nature of the FP distribution and the very great altitude reached by the balloons greatly reduces the magnitude of this extrapolation.

Table II shows the FP intensities measured on the various flights at 15 g/cm² and 5 g/cm² and the corresponding extrapolated primary proton intensity (plus re-entrant albedo). At this time it is not possible to isolate the returning albedo. However, in Sec. VIII

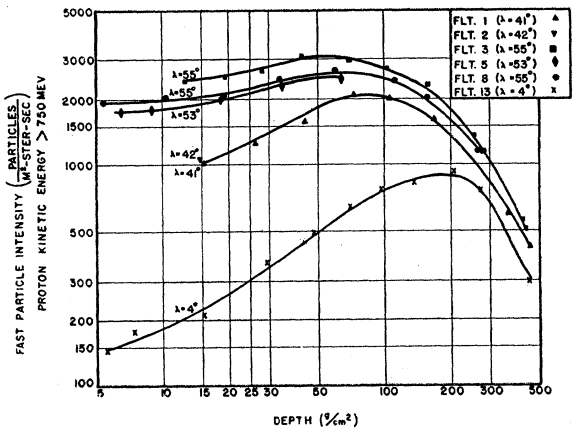

FIG. 7. Altitude dependence of the fast-particle intensity (corrected for background events) at various latitudes. The fast particles have $\beta \geqq 0.83$ (proton kinetic energy >750 Mev).

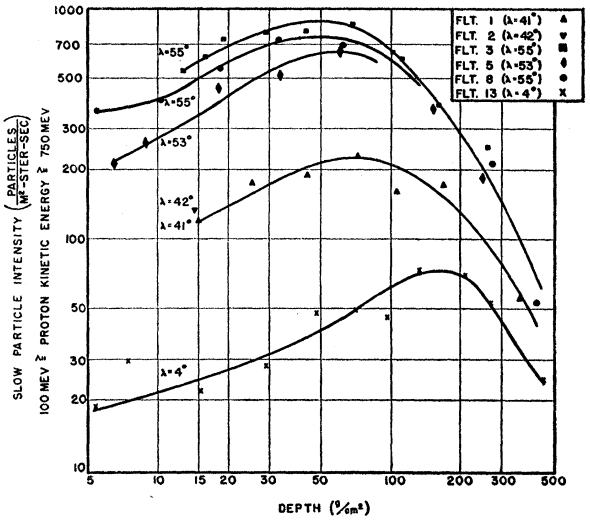

(a)

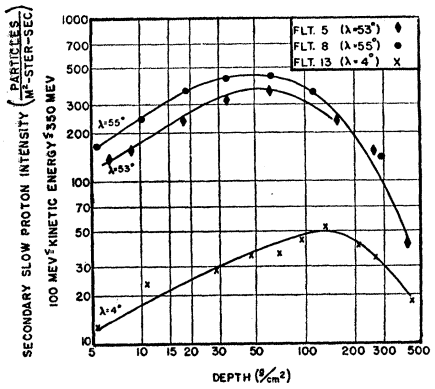

(b)

FIG. 8. (a) Altitude dependence of the slow-particle intensity (corrected for background events) at various latitudes. These counts correspond to protons in the energy range, 100 Mev $\leqq E_p \leqq$ 750 Mev, and include primaries as well as both upward and downward secondary particles. (b) Altitude dependence of slow secondary particles in the proton kinetic energy interval, 100 Mev $\leqq E_p \leqq$ 350 Mev. The primary protons present on Flight 8 in this energy interval have been subtracted.

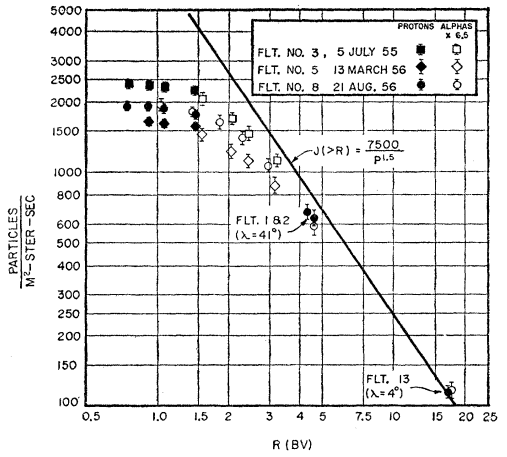

FIG. 9. Integral intensity-rigidity spectrum for primary protons. The alpha-intensity data, multiplied by a factor of 6.5, from the same flight are also shown. No correction has been made for returning fast albedo particles.

upper limits will be set on the amount of returning albedo.

The intensities in Table II have been plotted in Fig. 9 as a function of rigidity. Also plotted in Fig. 9 are the alpha-particle intensities measured on the same flights multiplied by 6.5. The integral number rigidity spectrum $N(>R)7500/R^{1.5}$ fits the data (quite accurately) in the region 5–15 Bv. It is clear that large changes have occurred in the low-rigidity component of the primary radiation during the time interval in which the flights were conducted, thus making the concept of such a simple rigidity spectrum of little value in the region below 5 Bv. A more detailed analysis of the low-rigidity end of the proton spectrum and its comparison with the alpha-particle spectrum will be considered in Sec. IX.

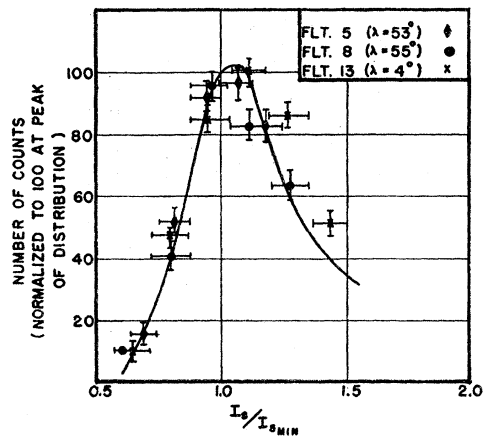

FIG. 10. Scintillation-counter distribution for fast splash albedo particles.

VIII. INTENSITY AND COMPOSITION OF FAST SPLASH ALBEDO

The intensity and pulse-height distributions of the fast splash albedo have been examined carefully for three flights, flight 13 ($\lambda=4°$), flight 5 ($\lambda=53°$) and flight 8 ($\lambda=55°$). These flights were chosen because they reached very high altitudes and because the separation of the FSA counts was especially good (see Fig. 5). This improvement in the resolution obtained on these later flights was accomplished by decreasing the reflectivity of the top side of the Čerenkov counter. The pulse-height distributions obtained are shown in Fig. 10. The solid curve represents the pulse-height distribution to be expected from $\beta\sim1$ albedo particles as measured by inverting the apparatus at sea level.

The data from all three flights are consistent with a fast splash albedo composed largely of $\beta\sim1$ particles. This rules out protons (and to a lesser extent mesons) as being a major component in the FSA. If there were large numbers of protons (or mesons) in the FSA, one would not expect the pulse-height distribution to be so sharply peaked about $I_{s\,\min}$ since the energy distribution of these secondary protons would be such as to give a wide range of energy losses (I_s). In fact, most of the protons would be expected to have a much greater energy loss. We must then conclude that the FSA consists primarily of electrons with a range >10 g/cm^2. The data on the intensities of the FSA are given in Table III. It is found for all the flights that the intensity of FSA rises steadily in the region 500–50 g/cm^2, leveling off at about 50 g/cm^2 and remaining constant up to the highest altitudes reached. We can thus reasonably assume that the intensity of FSA measured on these flights represents the intensity of these particles at the top of the atmosphere. The $\lambda=55°$ and 53° data are in good agreement with the results of Anderson.[11] The $\lambda=4°$ data are significantly lower than his values.

It is evident that a large fraction of this splash albedo will return to the atmosphere as re-entrant albedo. The detector used in this experiment is unable to distinguish these particles from the primary protons. However, because of the uncertainty in the fraction of the splash albedo that will return to the atmosphere as re-entrant albedo, we have not attempted to correct the primary

TABLE III. Albedo intensities near the top of the atmosphere.

Flight number	Intensity of fast splash albedo at 5–6 g/cm² in particles/m²-sec-sterad	Intensity of FSA at 0 g/cm² in particles/m²-sec-sterad	Intensity of albedo (splash + re-entrant) protons, 100 Mev $\leqq E_p \leqq$ 350 Mev at 0 g/cm²
Flt. 13 ($\lambda=4°$)	22±2	22±2	6±3
Flt. 5 ($\lambda=53°$)	84±8	84±8	30±15
Flt. 8 ($\lambda=55°$)	89±8	89±8	40±15

[11] K. A. Anderson, Suppl. Nuovo cimento **5**, 389 (1957).

TABLE IV. Determination of the low-rigidity end of the differential rigidity spectrum for primary protons.

Flight No.	Excess over normal slow-proton energy distribution in particles/m²-sec-sterad at 6 g/cm²			Particles/m²-sterad-sec-Mev/c corrected to top of atmosphere (dJ/dp)		
	250–350 Mev	350–500 Mev	500–750 Mev			
5 ($\lambda=53°$)				730–870 Mev/c	870–1110 Mev/c	1110–1450 Mev/c
(1)	...	...	...	...	...	...
(2)	...	...	26±7	...	...	0.08±0.02
(3)	...	30±7	74±12	...	0.11±0.03	0.25±0.05
3 ($\lambda=55°$)(A)	20±4	41±8	80±12	0.15±0.04	0.23±0.04	0.34±0.05
8 ($\lambda=55°$)(B)	7.0±3	30±7	75±12	0.05±0.02	0.12±0.04	0.23±0.04

intensities in Table II for this effect. The FSA intensities are believed to represent a reasonable upper limit on the amount of returning albedo.

As has been pointed out previously, it is impossible to tell the direction of particles with $\beta<0.7$ (i.e., protons with $100\leq E\leq 350$ Mev). It is possible to separate the secondary protons from the albedo protons (splash +re-entrant) in this energy range in the following manner, however.

We first plot the intensity of SP in the energy range 100–350 Mev [Fig. 8(b)] as a function of altitude [correcting the flight 8 ($\lambda=55°$) for the presence of primaries in the range 250–350 Mev]. In the absence of splash + re-entrant albedo in this energy range these curves should extrapolate to zero at the top of the atmosphere. In all cases they extrapolate to some small value which is here taken to be the intensity of splash plus re-entrant albedo in this energy range at the top of the atmosphere (see Table III). This proton component of the albedo will be observed as a rapidly absorbed portion of the primary radiation at extreme altitude but can clearly be distinguished from the primary radiation in this experiment.

IX. SLOW PROTONS AND THE LOW-RIGIDITY END OF THE PRIMARY PROTON SPECTRUM

The energy spectra for protons in the energy range $100\leq E_p\leq 750$ Mev at maximum altitude (5–15 g/cm²) are shown in Fig. 11 for all flights. The data for the various flights are normalized in the region $100\leq E_p\leq 250$ Mev. Note that these spectra are the same at all latitudes except for the high-latitude flights, Flight 3 and 8 ($\lambda=55°$) and a portion of Flight 5 ($\lambda=53°$) which show an excess of counts in the energy range 250–750 Mev. This excess of counts is interpreted to be due to primary protons arriving in this energy range on these flights. This is particularly noticeable in Flight 5 which passed over about 2° of geomagnetic latitude. The low energy distribution was normal at the start of the ceiling altitude portion of the flight, indicating the geomagnetic cutoff was >750 Mev. By the end of the flight, however, particles were arriving down to 380 Mev.

The energy distribution of slow protons has also been obtained as a function of atmospheric depth. At depths greater than 50 g/cm² the energy spectra for all flights become the same. This is so because the intensity of secondary protons increases, while the primaries interact and are degraded in energy and hence become relatively less abundant. At 150 g/cm² the differential energy distribution of the secondary protons has developed a peak at about 200 Mev corresponding to the equilibrium condition between ionization loss and production of the low-energy protons.[12]

The solid curve of Fig. 11 represents the energy spectrum of secondary protons at high altitudes (5–15 g/cm²) and all latitudes.

Table IV lists the excess intensities of slow protons in the energy range 250–750 Mev observed on the three high-latitude flights and attributed to primary protons. From these intensities the differential rigidity spectra for primary protons at the top of the atmosphere are determined for each of the three flights and are shown in Fig. 12.

The assumption that is made when one uses this method is that the energy spectra of low- and medium-energy protons from stars are independent of the kinetic energy of the initiating particle. Thus if the proton data from all flights are normalized in the 100–250 Mev regions, the same spectrum should be obtained at all latitudes unless there are primary protons with kinetic energy less than 750 Mev, and these will appear as excess counts. That this indeed is a valid method is

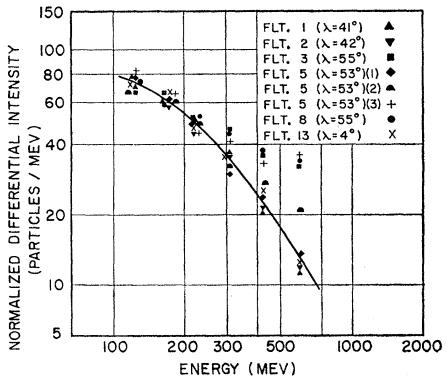

FIG. 11. Differential number-energy spectrum for protons with $100\leq E_p\leq 750$ Mev at 5–15 g/cm².

[12] B. Rossi, *High-Energy Particles* (Prentice-Hall, Inc., New York, 1952), p. 438.

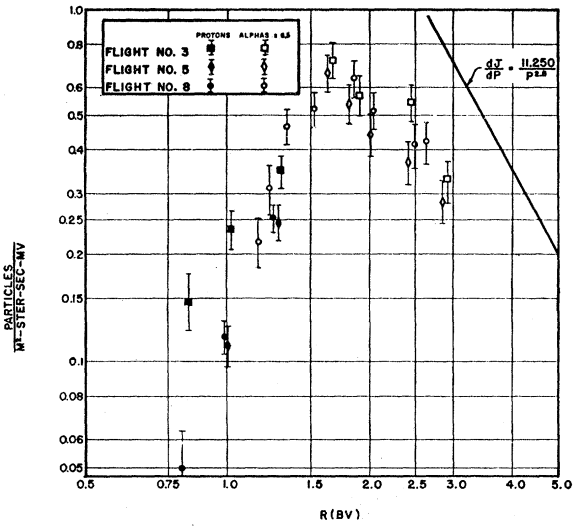

FIG. 12. Direct determination of low-rigidity portion of the primary differential rigidity spectra for protons and alpha particles as measured on three high-latitude flights. The alpha data has been multiplied by a factor of 6.5.

well confirmed by the excellent agreement obtained between flights at $\lambda=4°$, 41°, and 53° where the cutoff energy was >750 Mev. Such an assumption is in agreement with the results of Camerini *et al.*,[7] who report that the average energy of grey tracks (corresponding to protons in energy interval 60–500 Mev) is independent of primary energy when the primary energy is >1 Bev and is a very slowly varying function of primary energy down to 0.3 Bev.

The detailed data from Flight 5 ($\lambda=53°$) further verify the reality of the low-energy particles and offer additional proof that the method of analysis is a valid one. As previously mentioned, when this flight reached ceiling altitude, no primary protons below 750 Mev were observed. However, as the flight moved north through 2° of geomagnetic latitude, protons of energy down to 380 Mev appeared and the primary energy spectrum of the additional primary protons was in good agreement with that measured at 55°.

The proton energy spectrum of Flight 8 ($\lambda=55°$) was also obtained by another method. On both Flight 8 and Flight 5 ($\lambda=53°$) identical equipment was used and the ceiling altitudes agreed within 1 mb. From Table II we note that the flux of fast primaries on Flight 5 is 12% less than on Flight 8. This is used as the normalization factor for the complete two-dimensional array of counts on the ceiling altitude portion of Flight 5 where the measured cutoff is greater than 750 Mev. The normalized Flight 5 data were then subtracted from those of Flight 8 leaving residual counts in the 250–750 Mev region for Flight 8. These counts were corrected for Landau fluctuations and the resulting proton energy spectrum deduced for Flight 8 was identical to that obtained by the low-energy normalization method. The proton data included in Fig. 12 are also summarized in Tables II and IV.

Also shown in Fig. 12 are the differential rigidity spectra for alpha particles observed on the same flights. (Note that the α intensities have been multiplied by a factor of 6.5.) It is immediately obvious that it is far more meaningful to compare the differential rigidity spectra than the differential energy spectra of the two components. The remarkable similarity of the spectra of these two components when plotted in this manner can be clearly seen. In Fig. 9 it is observed that the integral rigidity spectra are also in excellent agreement at all latitudes covered in this survey when the alpha intensity is multiplied by 6.5. The excellent agreement of the integral rigidity spectra in the region 1.3 Bv to 17 Bv and the differential rigidity spectra in the range 1 to 1.5 Bv implies that cosmic-ray primary protons and alphas must have very nearly the same form of rigidity spectrum in the region 1 to 17 Bv. This also suggests that the mechanism which is producing the peak in the primary differential spectrum is a rigidity-dependent one as it affects the two components similarly. In addition, there are systematic changes in the differential rigidity spectra for the various components among the three high-latitude flights which are consistent with corresponding changes in the integral spectra and which further suggest a rigidity-dependent mechanism is responsible for these changes.

The above proton differential rigidity spectrum extends to 0.8 Bv. The data obtained by Winckler and Anderson[13] and by Neher[14] at higher latitudes during the summers of 1954–55 would seem to indicate that the spectrum measured at $\lambda=55°$ cannot be extended to much lower rigidities but must, at least at these particular times, indeed rise as one goes to lower energies if the particles counted by Neher, Winckler, and Anderson were primary protons.

X. DETERMINATION OF CUTOFF RIGIDITIES

It is evident that the above analysis enables one to determine the cutoff rigidities for primary protons for the high-latitude flights. The cutoff rigidities over the north central United States as deduced from both proton and alpha particle measurements are shown in Table V. In passing over 2° geomagnetic latitude [see Fig. 4(b)] the cutoff rigidity on Flight 5 changed from >1.5 Bv to 0.9 Bv. The proton cutoff rigidities measured on these flights are in good agreement with comparable measured α-particle cutoff rigidities of Freier, Ney, and Fowler,[15] and McDonald.[16]

These measured cutoff rigidities are in substantial disagreement with those expected from a simple dipole

[13] J. R. Winckler and K. A. Anderson, Phys. Rev. **108**, 148 (1957).
[14] H. V. Neher, Phys. Rev. **107**, 588 (1957).
[15] Freier, Ney, and Fowler, Nature **181**, 1319 (1958).
[16] F. B. McDonald, Phys. Rev. **107**, 1386 (1957).

TABLE V. Measured cutoff rigidities for protons and alpha particles.

Flight +int. No.	Mean geographical position of flight or selected interval[a]	Measured proton cutoff rigidity and energy $R_{p\,\min}$	$E_{p\,\min}$	Corresponding alpha cutoff energy implied by proton measurements, $E_{\alpha\,\min}$	Measured alpha cutoff energy[b] $E_{\alpha\,\min}$
Flt. 3 ($\lambda=55°$)	45° 09′ N, 95° 20′ W	0.71±0.06 Bv	250±30 Mev	75 Mev/nuc	Not measured
Flt. 8 ($\lambda=55°$)	44° 41′ N, 94° 51′ W	0.81±0.07 Bv	300±40 Mev	90 Mev/nuc	<150 Mev/nuc
Flt. 5 ($\lambda=53°$)					
Int. 1	42° 06′ N, 86° 40′ W	>1.4 ±0.09 Bv	>750±80 Mev	>225 Mev/nuc	}
Int. 2	42° 50′ N, 82° 35′ W	1.33±0.09 Bv	670±70 Mev	210 Mev/nuc	}220 Mev/nuc
Int. 3	42° 20′ N, 77° 40′ W	0.93±0.08 Bv	380±40 Mev	114 Mev/nuc	}
Flt. 6	42° 36′ N, 88° 09′ W	Not measured		···	225±25 Mev/nuc

[a] See Fig. 4(b) for trajectories. [b] See reference 15.

field but are in close agreement with those predicted by Rothwell[17] and by Quenby and Webber.[9] The close agreement is achieved by considering the effects of higher order terms in the earth's potential on the cutoff rigidities.

XI. TIME VARIATIONS OBSERVED ON THREE HIGH-LATITUDE FLIGHTS

Flight 5 ($\lambda=53°$) and Flights 3 and 8 ($\lambda=55°$) were made over a period of about a year and showed remarkable variations in intensity of both the proton and alpha-particle components of the cosmic radiation. Flight 3, made on July 7, 1955, occurred during a quiet period of solar activity just after sunspot minimum. Flight 8, made on August 21, 1956, occurred during a period of moderate 27-day cycles as recorded by sea-level neutron monitors. The general level of solar activity was also high. Neutron data indicated a pronounced long-term decrease in intensity from the 1954–55 solar minimum. Flight 5, made on March 13, 1956, occurred during a period of pronounced solar activity and was at the bottom of a large Forbush type decrease. A long-term decrease in intensity from 1954–55 was also evident from neutron monitor data. In addition, an "enhanced" daily variation was also observed this day at various North American neutron stations. This was strikingly reflected in the flight data.[16]

The July 7, 1955 flight has been chosen as a "normal" flight, corresponding to a period of low solar activity near sunspot minimum. The percentage changes in intensity from July 7 for both protons and alphas (both integral and in various differential rigidity ranges) are shown for the August 21 and March 13 flights. Corresponding changes in intensities recorded by the Climax and Huancayo neutron monitors are also shown in Table VI for these days.[18]

The changes occurring between July 7, August 21, and March 13 (*I*) consist primarily of (1) long-term variations (11-year cycle) and (2) 27-day or cosmic-ray storm (Forbush decrease) variations. It is not possible to separate completely the relative influences of the two types of variations responsible for these changes, however the storm effect is believed to be the most important factor in the lowered intensity on interval *I*, Flight 5, March 13 with the long-term variation the most important factor in the lowered intensity on August 21. Thus, if the modulating mechanisms responsible for the two types of change have a widely differing rigidity dependence, it seems reasonable to suppose that the rigidity dependence for the changes between the three flights should also be different. Within experimental error this is not observed.

If indeed the modulating mechanisms responsible for the two types of change [i.e., (1) 11-year change, (2) cosmic-ray storm/27-day change] do have similar rigidity dependences the question then arises: can one project a simple rigidity dependence that will produce the observed changes? Obviously the rigidity or energy dependence of the change may be arbitrarily complex

TABLE VI. Correlations between time variations of the primary radiation and neutrons at mountain altitudes.[a]

Flight	Huancayo	Climax	Protons $R>1.45$	Protons $1.1\leq R\leq 1.45$	Protons $0.8\leq R\leq 1.1$	Alpha $R>1.45$	Alpha $1.45\leq R\leq 3.2$
July 7, 1955 (base period)	1329	3324	2240	110	48	305	107
Observed long-term and 27-day storm variations: Aug. 21, 1956	−0.8%	−4.4%	−18.5±2%	−31±8%	−43±12%	−12.5±4%	− 8.0±8%
Observed long-term and 27-day storm variations: March 13, 1956 (I)	−2.3%	−7.8%	−29.0±2%	···	···	−28.5±4%	−18.0±8%
Predicted long-term and 27-day storm variations: Aug. 21, 1956	−1.2%	−4.4%	−14%	−32%	−41%	−14%	−21%
Predicted long-term and 27-day storm variations: March 13, 1956 (Int. I)	−2.1%	−7.8%	−26%	···	···	−26%	−38%

[a] Percentages are expressed as differences from base period. Predicted changes are normalized to observed changes in climax neutrons.

[17] P. Rothwell, Phil. Mag. **3**, 961 (1958).

[18] The authors want to thank Dr. J. A. Simpson of the University of Chicago for making these and other neutron data available to them.

and we cannot proceed in a straightforward manner to deduce it from the limited experimental data. We suggest, however, the somewhat artificial form $dJ(t)/dR = (dJ_0/dR)[1-K(t)/R]$ for the modified differential spectrum. Using such a modified spectrum in conjunction with revised yield functions for the nucleonic component,[19] one can calculate the particular changes to be expected corresponding to changes in Climax neutrons. These changes are given in Table VI. Note the very satisfactory agreement between the observed percentage changes in the proton component and calculated changes over the rigidity range from 15 Bv to 1 Bv. The observed integral alpha-particle intensity changes are also in agreement with these calculations. The decrease of alpha particles in the range $1.5 \leqq R \leqq 3.2$ Bv is smaller than predicted, however. In fact, from the observed decrease of alpha particles in this rigidity range we must conclude that the high-rigidity alphas changed *more* than the low-rigidity ones. However, the statistical accuracy of the alpha-particle data is not good enough to establish this fact with certainty.

We note, in addition, that the suggested rigidity dependence of the modulating mechanism which will explain the results obtained on our flights will also predict a latitude effect for the amplitude of the 11-year cycle of approximately 4:1 for nucleon detectors near sea level. This ratio is actually observed during the current 11-year cycle.[20,21]

If we assume the cosmic-ray storm/27-day modulating mechanism exhibits the same rigidity dependence, then we should also expect the same latitude effect for this type of variation. However, if we assume that the modulating mechanism responsible for this effect acts on a primary spectrum which has *already* been modulated by the mechanism responsible for the 11-year cycle, then this ratio should be less than 4:1 for neutron monitors and in fact variable (from approximately 2.5:1 to 4:1) with the solar cycle. A latitude effect of this magnitude and its variation with the solar cycle have also been observed.[21]

It is of interest to see whether the rather specific rigidity dependence of the modulating mechanisms which our data imply and which are in agreement with detailed analysis of neutron variations can be explained by any of the modulating mechanisms in current favor. We shall only consider mechanisms for which specific calculations of the rigidity or energy dependence have been made.

For the 11-year cycle two such mechanisms have been suggested. (1) A solar cavity model introduced by Davis[22] and upon which specific calculations of the rigidity dependence of the changes have been carried out by Beiser.[23] In this model ion streams emitted by the sun are assumed to push back the lines of force of the galactic magnetic field, creating a nearly field-free cavity around the sun. Low-energy cosmic-ray particles moving along galactic lines of force are then unable to penetrate into the inner solar system.

(2) A quasi-stationary region of disordered magnetic fields surrounding either the earth[24] or the sun.[25,26] Cosmic rays will tend to diffuse inward through this shell with equilibrium being reached when the rate of diffusion inwards is equal to the rate at which they are absorbed in the interior. Thus the cosmic-ray intensity inside the shell is less than outside.

The mechanism of a disordered magnetic field surrounding the earth has also been used[24,27] to explain the cosmic-ray storm or Forbush-type decrease. All of these mechanisms predict in a qualitative way a peak in the primary differential spectrum and consequently the appearance of a "knee" in the cosmic-ray latitude curve. However, in all cases, the specific rigidity or energy dependence of the cosmic-ray changes predicted by these authors is substantially different from that suggested by our results.

Quantitative calculations on the changes in intensity to be expected when a rapidly moving beam or jet of ionized gas carrying a magnetic field outward from the sun passes near the earth have also been carried out by Dorman.[28]

This mechanism, originally suggested by Alfvén,[29] has been used by Dorman to explain Forbush decreases. The energy dependence of the changes derived by Dorman are considerably different from those suggested by our results.

Finally, we should mention the uniform deceleration of cosmic rays by an electric field as suggested by Nagashima.[30] This electric field may be a geocentric mechanism or perhaps even a heliocentric one. Its effect would be to shift the energy of each incoming particle by a fixed amount. The actual form of the change in the primary spectrum is given by the expression

$$\frac{dJ_e}{dE}(E-V) = \frac{dJ_\infty}{dE}(E)\left[\frac{(E-V)(E-V+2)}{E \quad (E+2)}\right],$$

where $(dJ_e/dE)(E-V)$ is the differential flux value at the earth of particles with kinetic energy $E-V$. $(dJ_\infty/dE)(E)$ is the differential flux value at large distances from the earth (region of $V=0$) of particles with kinetic energy E. V is the decelerating potential.

[19] W. R. Webber and J. J. Quenby, Phil. Mag. (to be published).
[20] S. E. Forbush, Report of American IGY Work given at CSAGI Conference, Moscow, 1958.
[21] K. G. McCracken *et al.*, Report of IGY Work at Hobart given at CSAGI Conference, Moscow, 1958.
[22] L. Davis, Phys. Rev. **100**, 1440 (1955).
[23] A. Beiser, J. Geophys. Research **63**, 1 (1958).
[24] E. N. Parker, Phys. Rev. **103**, 1518 (1956).
[25] Meyer, Parker, and Simpson, Phys. Rev. **104**, 768 (1956).
[26] E. N. Parker, Phys. Rev. **110**, 1445 (1958).
[27] R. R. Brown, Nuovo cimento **9**, 197 (1958)
[28] L. L. Dorman, *Cosmic-Ray Variations* (State Publishing House for Technical and Theoretical Literature, Moscow, 1957).
[29] H. Alfvèn, *Cosmical Electrodynamics* (Clarendon Press, Oxford, 1950).
[30] K. Nagashima, J. Geomag. Geoelec. **5**, 141 (1953).

At large values of R, assuming a power law spectrum, the expression for the electric field modulation reduces to

$$\frac{dJ}{dR}(R)=\frac{dJ_0}{dR}(R)\left[1-\frac{K(t)}{R}\right],$$

where $K(t)=\text{const}\times V$.

In other words above approximately 2.5 Bv it is impossible to distinguish a mechanism with constant energy loss per particle such as an electric field from the rigidity dependent formula we have proposed. The electric field model should give a splitting of the low energy proton and alpha differential spectra but the values of V are too small for this to be observable in these experiments. The results of our experiment are then consistent with an electric field deceleration mechanism—both as the cause of the long-term effects and as the cause of the Forbush decreases. However, it is difficult to visualize electric fields, such as are necessary to produce the desired cosmic-ray effects, existing in the inner solar system using the conductivities that are presently accepted. We want to emphasize strongly that we have considered only those proposals wherein the authors have calculated the rigidity or energy dependence to be expected from their models. It is possible that these models might be modified to bring the prediction into closer agreement with experimental observations.

XII. DISCUSSION

The Čerenkov-scintillator technique provides an accurate and reliable method for the determination of primary proton intensity values. The equatorial intensities determined by this technique are appreciably lower than those obtained by other experiments (see reference 10 for a complete comparison of proton flux when near $\lambda=0$). However, this appears to be the first experiment in which an accurate extrapolation to the top of the atmosphere can be made and where the effects of splash albedo and slow secondaries are adequately taken into account. The proton intensity measured at $\lambda=41°$ is in good agreement with the rocket value obtained by Perlow[1] in February, 1950, at this same latitude. The intensity measured at $\lambda=55°$ in August, 1956, agrees well with the values obtained by Davis *et al.*[2] at this same latitude in 1952, two years before solar minimum.

The intensity of fast splash albedo was accurately determined on three flights of the series. The tentative identification of electrons as the principal contribution to the fast albedo is consistent with the results of Perlow[1] and Davis.[2]

The Čerenkov-scintillator technique provides for the first time a direct determination of the low-energy (100–750 Mev) primary proton differential energy spectrum. These measurements, when compared with similar ones for alpha particles on the same flights, strongly indicate that primary cosmic-ray protons and alphas have the same differential rigidity spectra over the entire range from 1 to 17 Bv. These measurements show conclusively that these two components exhibit the same form of rigidity dependence as opposed to a similar energy dependence. The results also indicate that the so-called "cutoff" producing the latitude knee is not sharp but is simply produced by a gradual "turning over" of the differential spectra. These results are in agreement with the results of Meredith *et al.*[32] on the behavior of the low-rigidity portion of the proton differential spectra in 1952. However, their conclusion that the cutoff appeared to be sharp should be modified in the light of our findings.

The results of Neher[14] and also Winckler and Anderson[13] show a latitude effect exists for the total radiation at balloon altitudes near solar minimum even at latitudes with cutoff rigidities <0.75 Bv (e.g., $\lambda>60°$). If these additional particles are primary protons, our observed differential spectra cannot be extrapolated directly to rigidities below 0.75 Bv. We must assume then that great changes occur from day to day in this low rigidity region of the primary spectrum even during solar minimum (not observed by Neher) or that perhaps a new influence is taking place in this low rigidity region (e.g., additional "nonprimary" particles).

The cutoff energies for protons measured in this experiment are in good agreement with comparable measurements on alpha particles by Fowler *et al.*[15] and McDonald.[16] They indicate quite clearly that the centered dipole approximation is no longer adequate to predict geomagnetic cutoff rigidities. However, consideration of the higher order terms of the earth's magnetic potential as determined by the earth's surface field can explain the experimental results.[9,17]

The time variation data are scanty, but very revealing. Flight 3 was regarded as a normal quiet day flight near the minimum of solar activity. Subsequent flights, during a variety of superimposed decreases, revealed a strong rigidity dependence. An empirical formula, $dJ(t)/dR=(dJ_0/dR)[1-k(t)/R]$, was found to agree with the observed changes in the proton and alpha intensities. None of the proposed modulation mechanisms where a specific rigidity or energy dependence has been calculated are in agreement with the observations with the exception of the electric field deceleration proposed by Nagashima.[30] At the present time the existence of such a large electric field within the solar system appears to be unreasonable.

ACKNOWLEDGMENTS

The authors wish to thank the Office of Naval Research for the excellent Skyhook balloon flights they provided.

[32] Meredith, Gottlieb, and Van Allen, Phys. Rev. **97**, 201 (1955).